

## Setting boundaries on the recipe for a successful RbF post-deposition treatment of CIGS

Lorelle M. Mansfield,\* Stephen Glynn, Steve Johnston, Craig Marshall, Christopher P. Muzzillo, Bart Stevens, Matthew R. Young

\*Corresponding author

National Renewable Energy Laboratory, 15013 Denver W Pkwy, Golden, CO 80401, USA

### Abstract

RbF post-deposition treatments have been explored in the literature for increasing the open-circuit voltage, fill factor, and hence the efficiency of Cu(In,Ga)Se<sub>2</sub> solar cells. However, given the few papers documenting the experimental steps, it was difficult to quickly reproduce the results. This contribution describes some of the optimization steps that led to a successful RbF PDT based on device performance. We present results that put boundaries on the temperatures of the RbF cell and the lamp (for sample heating) setpoint. The best recipe for our specific growth process is documented in detail so that others may copy the procedure and possibly arrive at a successful RbF PDT in a reasonable time.

### 1. Introduction

RbF post-deposition treatments (PDTs) have been explored in the literature for increasing the open-circuit voltage ( $V_{oc}$ ), fill factor (FF), and hence the efficiency of Cu(In,Ga)Se<sub>2</sub> solar cells [1,2]. One study of several alkali fluoride PDTs found that diode quality improved with the heavy-alkali PDTs (RbF or CsF) over KF PDTs [1], whereas another concluded similar performance for RbF and KF PDTs [2]. After successfully implementing KF PDTs on CIGS absorbers that were coevaporated using the 3-stage process, using constant elemental fluxes [3], processed by two-step precursor/selenization [4], and previously grown by NREL and other organizations [5], we expected that implementing and optimizing a RbF PDT would be a relatively quick and easy process. However, it took longer than expected, and our RbF PDT parameters did not match those documented in the literature.

Some of the most descriptive RbF PDT parameters found in the literature are listed in Table 1 in order of ascending publication date. Columns 1 through 5 require sufficient information to successfully repeat the RbF PDT. Variation exists in the number of parameters reported. For the recipes shown here, sample temperatures in column 1 range from 220 to 350 C. That would suggest a wide process space for successful RbF PDT. Column 2 is comprised of RbF parameters, but not all of them are needed to define a given recipe. For example, combinations of RbF Flux plus RbF Time or RbF Cell Temp plus RbF Time are two ways to fully describe the RbF deposition. Se rate during the RbF PDT (column 3) was not explicitly stated in any of the recipes shown here. That could be because having an exact Se flux is not as important as the other parameters. CIGS samples with RbF PDTs are often rinsed before depositing the next layer in the cell stack, especially if the next layer is fabricated via chemical bath. Rinse solutions and times (columns 4 and 5) varied somewhat, with ammonium hydroxide solutions being the most popular rinse solution. All these differing parameters led us to a several-month investigation and optimization of the RbF PDT process.

Table 1. Published RbF PDT Parameters

Author [Ref]	Absorber Processing Method	1.	2. RbF Deposition			3.	4.	5.	From
		Sample Temp (°C)	RbF Cell Temp (°C)	RbF Flux	RbF Time or Dose	Se Rate	Rinse Solution	Rinse Time	
Anvancini [2]	Multi-stage evaporation			1-2 nm/m	20 min		2 M NH <sub>4</sub> OH	1 min	EMPA
Ishizuka [6]	Three-stage coevaporation	350	560 to 620		10 min	Yes	No		AIST
Weiss [7]	Low temp coevaporation	220 to 250	460 to 550		20 min		H <sub>2</sub> O or HCl	20 s to 5 min	EMPA
Kodalle [8]	Multi-stage evaporation	280		0.2 Å/s	10 min	Yes, reduced	NH <sub>3</sub> (aq) (1 mol/l)		HZB
Karki [9]	Three-stage process	350			10-20 nm	Yes	2N NH <sub>4</sub> OH	1 min	ODU

## 2. Experimental

NREL's basic device fabrication procedures have been enumerated previously, and here is a brief review. CIGS absorbers were deposited on Mo-coated soda-lime glass substrates. The three-stage process was used to produce high-quality CIGS material [10]. PDTs, if used, were performed immediately after the CIGS deposition (more details in section 2.2). CIGS films were processed into devices using our standard layers: 50 nm of CdS [11] was followed by bi-layer ZnO (90 nm i-ZnO then 120 nm ZnO:Al) and 50 nm Ni plus 3 μm Al for grids [12]. The devices were isolated by photolithography and etching, resulting in 0.42 cm<sup>2</sup> solar cells. Anti-reflective coatings were not applied to any of these devices.

Current density – voltage (J-V) measurements were performed under 1000 W/m<sup>2</sup> AM1.5G illumination on a 25°C temperature-controlled stage. Secondary ion mass spectrometry (SIMS) was performed on representative ammonia-rinsed absorber stacks to obtain elemental depth profiles. Rb count profiles were converted into absolute concentrations by using calibration standards. Current – voltage – temperature (IVT) measurements were performed in a cryostat with temperature range of 84K to 300K. At each temperature, voltage was swept from -0.4 V to 1.5 V.

### 2.1 Post-deposition Treatment

NREL previously implemented a successful KF-PDT process. The parameters were arrived at through a 3-factor, 3-level design of experiments (DoE) which is a statistically structured and efficient approach for optimizing processes. In our KF recipe, the substrate lamp temperature was set to 370°C for a 15-minute dwell time. The KF cell temperature was 685°C. For quick reference, our KF PDT parameters are listed in Table 2.

Table 2. NREL KF PDT Parameters

Lamp Temp (°C)	Sample Temp (°C)	KF Cell Temp (°C)	KF Time (min)	KF Dose (nm)	Dwell Time (min)	Se Rate (Å/s)	Rinse Solution	Rinse Time (min)	Rinse Temp (°C)
370	353	685	6.5	30	15	35	1.6 M NH <sub>4</sub> OH	4	65

For RbF PDTs, the RbF was evaporated from an R21000 RADAK II source by Luxel with a type K thermocouple. The 10 cm<sup>3</sup> crucible was filled to between ¼ and 1/3 capacity. Before the first PDT deposition using new RbF, the RbF cell was slowly ramped in temperature, keeping the pressure in the chamber below 5e-5 torr while the new RbF charge outgassed over hours. After the pressure stabilized, the RbF cell temperature was increased until RbF flux rate was observed on a quartz crystal monitor. The distance between the top of the RbF cell and the substrate was approximately 30.5 cm. During depositions without PDTs, the RbF cell temperature was held at 400°C, a warming temperature that was low enough to prevent significant RbF evaporation during the CIGS deposition. The 400°C RbF cell temperature and the lower height of the RbF source compared to the Cu, In, Ga, and Se sources prevented the deposition of metals on the RbF source. The RbF crucible did not need frequent refilling and the RbF charge did not degrade with time. We tested for RbF degradation by completely replacing the RbF material in the crucible. No significant differences were found in the performance of devices made before and after the RbF replacement. Daytime humidity in the Golden, CO lab is low, generally less than 30%. That along with opening the vacuum chamber only for short periods of time also contributed to preventing RbF source degradation. Humid locations may experience challenges associated with the RbF source absorbing water, similar to the way samples do, as described in section 3.1.

Recipes for the investigation of RbF-PDT parameters had several similar characteristics. An example of deposition parameters is shown in Figure 1. Because the deposition system did not have a shutter, the RbF cell temperature ( $T_{\text{RbF}}$ ) was held at a warming temperature during the CIGS deposition; typically, 400°C. At the end of the 3<sup>rd</sup> stage of CIGS deposition,  $T_{\text{RbF}}$  was ramped up at 30°C/min to the final RbF cell temperature minus 90°C. After the 3<sup>rd</sup> stage, the substrate temperature was ramped down (21.5°C/min). When it reached the given lamp setpoint temperature ( $T_{\text{lamps}}$ ) the temperature ramp was interrupted and held at  $T_{\text{lamps}}$  for 9 minutes during the RbF PDT. In this deposition system, the actual substrate temperature is approximately 10°C lower than  $T_{\text{lamps}}$  in the RbF-PDT temperature range, though this difference increases slightly with increasing temperature (Figure 1). The Se rate was adjusted to be 25 Å/s for the 9-minute PDT duration and during any subsequent substrate temperature cool down to a lamp temperature of 300°C. At the end of the 4-minute RbF deposition time, the RbF cell was quenched by cutting its power. It was standard practice to alternate the fabrication of samples with and without PDTs. This prevented alkali build-up in the chamber and allowed comparisons between consecutive samples to verify process stability and evaluate improvements due to PDTs.

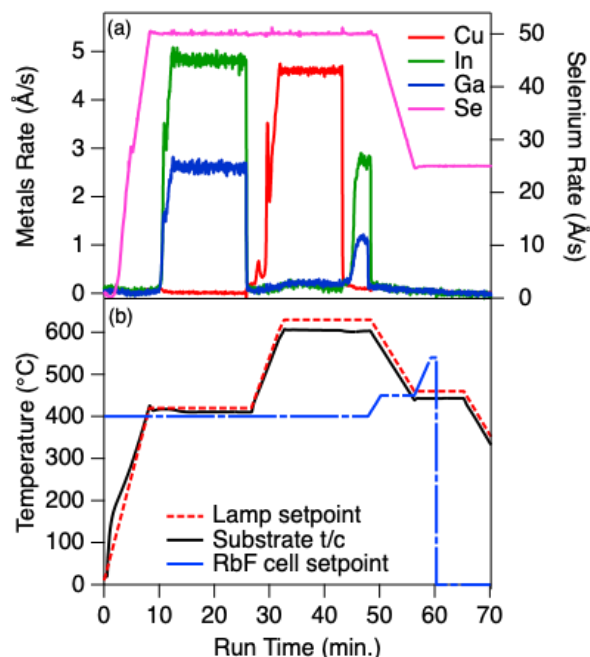


Figure 1. Example deposition parameters versus time. Elemental flux (a) has metal rates on the left axis and Se rate on the right axis. Setpoint temperatures (b) for lamps (red dash) and RbF cell (blue dash dot) along with substrate thermocouple (t/c) temperature (black).

## 2.2 Rinse Before CdS

All RbF-treated samples were rinsed before chemical-bath deposition of CdS. 12.5 ml of ammonium hydroxide was added to 100 ml of deionized (DI) water in a water-jacket beaker on a rocking platform. The temperature of the beaker was controlled by a circulating chiller set to 65°C. Samples were placed into the beaker immediately after the room-temperature solution, and the rocking platform was turned on. Samples were rinsed for 4 minutes, and then were removed and placed into a room-temperature DI water rinse momentarily while awaiting CdS deposition.

## 3. Results and Discussion

### 3.1 Challenges

We had difficulty measuring the amount of RbF that was deposited. Thin films are often deposited on masked substrates and then the thickness is measured with stylus or optical profilometry. RbF is hygroscopic, so it absorbs water easily from the air when removed from the deposition system. This made profilometry impossible without a controlled environment. Thus, we were not able to correctly set tooling factors on our quartz crystal monitors to measure the RbF deposition flux. Instead, we relied upon  $T_{\text{RbF}}$  and deposition time to control the RbF dose.

The RbF cell temperature was set to 590°C after the profilometry measurements. It seemed reasonable given the KF cell temperature and reference [6], but in hindsight it was too high. The KF PDT conditions listed in Table 2 were also considered when we began the RbF PDT

investigations. We did an initial 3-factor, 3-level DoE with substrate temperature setpoints of 300°C, 360°C, and 420°C. The RbF times used were 0 min, 4 min, and 8 min, and Se fluxes were 10 Å/s, 22.5 Å/s, and 35 Å/s. The best Rb-containing devices from this experiment had only 10% efficiency, which were lower performance than our baseline CIGS devices without any PDT. The reason for mentioning this failed experiment is that it led us to a few important conclusions. First, the Se flux rate was the least important factor that was varied. Second, the RbF time needed to be lower, meaning a lower dose of RbF. Since we already had short RbF deposition times, this indicated that the RbF cell temperature should be reduced for a lower dose of RbF. Third, the lamp setpoint temperature needed to be higher.

### 3.2 RbF PDT Parameter Space

The RbF PDT parameter space was explored by reducing the RbF cell temperature and raising the lamp setpoint temperature as indicated by initial experiments. The deposition procedure in the experimental section was followed with Se rate of 25 Å/s during the RbF PDT. Much of the parameter space that was explored is shown in Figure 2, where RbF cell temperature is on the y-axis and lamp setpoint temperature is on the x-axis. Each point (circle marker) represents at least one deposition run with those parameters. Several that are described in the text have a number to their right for easier location, and they will be referred to in the text using parentheses, such as (1). Table 3 lists parameters for the numbered cells. The color of each point corresponds to the maximum efficiency device out of at least 10 devices fabricated from CIGS depositions with the PDT conditions indicated on the axes. The purple color, corresponding to 17%, captures all devices with efficiencies of 17% or lower.

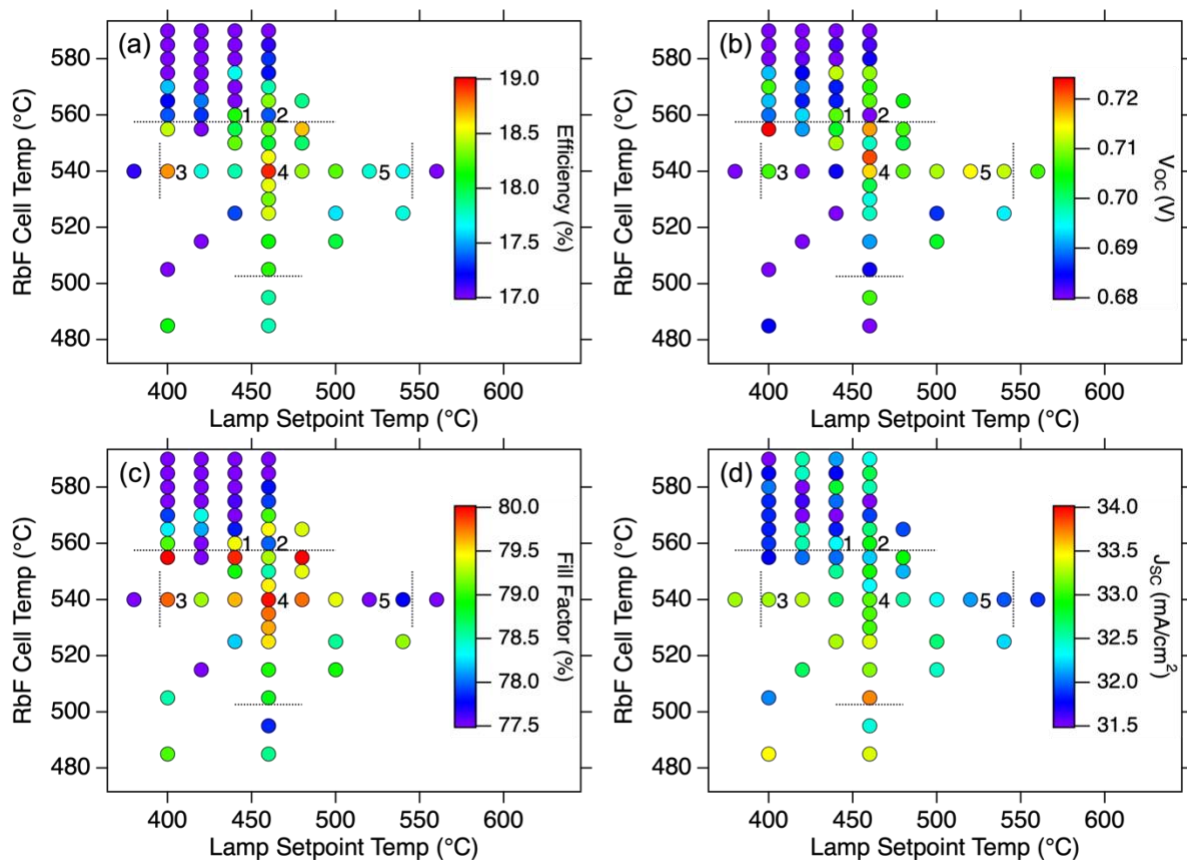


Figure 2. RbF cell temperature versus lamp setpoint temperature. Each point represents at least one deposition run with those parameters. Maximum efficiency a) for resulting devices is indicated by the color scale.  $V_{oc}$  b), Fill Factor c) and  $J_{sc}$  d) are shown for the same devices as in a). Purple points indicate that a given parameter is at or below the lower level indicated by the color bars. Successful RbF PDTs generally fall within the dotted lines. Points with a number to their right are described in the text.

Table 3. Parameters of Numbered Cells

Cell in Figure 2	RbF Cell Temp (°C)	Lamp Temp (°C)	Efficiency (%)	$V_{oc}$ (V)	$J_{sc}$ (mA/cm <sup>2</sup> )	Fill Factor (%)
1	560	440	18.2	0.708	32.3	79.4
2	560	460	17.4	0.677	32.9	78.0
3	540	400	18.7	0.707	33.2	78.8
4	540	460	18.9	0.716	33.1	80.0
5	540	520	17.8	0.714	32.1	77.4

Given the multitude of data points, it makes sense to put some boundaries on the parameters for a reasonable RbF PDT, given our deposition system and CIGS fabrication process. It is clear from the upper left points in Figure 2 that high RbF cell temperature, and hence high RbF dose, was detrimental to device performance. For some points in Figure 2, whether the RbF PDT was beneficial or detrimental was less clear. Because we are not running a production process, variability can occur between sets of runs. Our system accommodates one sample per run, must be opened to atmosphere

after each deposition, and is calibrated every week. It can go for weeks with excellent stable performance, or sometimes the baseline dips. To evaluate whether the RbF-PDT improved device performance, we calculated the percent change between device parameters of RbF-PDT samples and baseline samples (No PDT) that were deposited before and after the PDT sample. For example, the percent change in efficiency is  $\Delta\eta = \frac{\eta_{RbF} - \eta_{base}}{\eta_{base}} \times 100$ , where  $\eta_{RbF}$  is the efficiency of the RbF PDT device and  $\eta_{base}$  is the efficiency of the No PDT device. Both maximum and average values of parameters were considered. This led us to include some devices that were less efficient than their neighboring devices. For example, the two devices to the right of point (3) at  $T_{lamps}=420$  and  $440$  have lower efficiencies (17.7% and 17.8%) than points (3) and point (4). However, when compared to their baseline counterparts the average  $V_{OC}$ s are 15 mV and 35 mV higher, indicating that these RbF PDT conditions should be included within those that increase device performance. In cases where the percent change between baseline and RbF devices was small, JV curves were inspected. An example of JV curves is in Figure 3, where No PDT devices are red dashed lines and RbF PDT devices are blue lines. Figure 3(a) shows the JV curve from the RbF-PDT device at  $T_{RbF}=560$  and  $T_{lamps}=460$  (2 – point 2 in Figure 2) along with the JV curve from the No PDT device that was run right before it. The RbF-PDT device is not an improvement in this case. In contrast, the RbF PDT device (1) with  $T_{RbF}=560$  and  $T_{lamps}=440$  in Figure 3(b) shows an improvement over the No PDT device in both  $V_{OC}$  and FF. Those improvements translate into a 7.8% change in efficiency, or a 1.4% absolute efficiency increase.

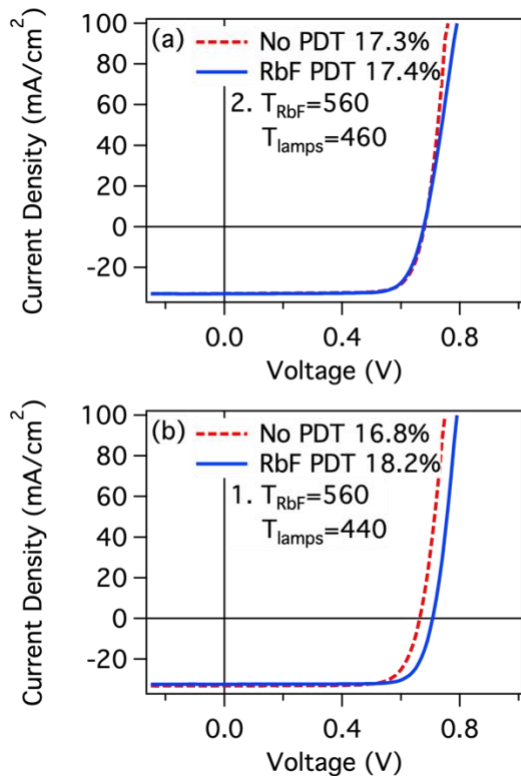


Figure 3. Sets of JV curves each comparing a RbF PDT sample (blue) to a sample without RbF (red dash). (a) shows the RbF sample at point 2 in Figure 2 and (b) shows point 1 which has a performance improvement over the No PDT device.

The most important factor affecting the success of an RbF PDT is the RbF dose, which is directly correlated to RbF cell temperature, so we consider it first. Looking at all devices in Figure 2 with  $T_{\text{RbF}} = 565^{\circ}\text{C}$ , for devices with  $T_{\text{lamps}} > 440^{\circ}\text{C}$  they are slightly better than related devices without RbF PDT. However, the maximum efficiency for  $T_{\text{RbF}} = 560^{\circ}\text{C}$  and  $T_{\text{lamps}} = 460^{\circ}\text{C}$  (2) is lower, and the only point with  $T_{\text{RbF}} = 560^{\circ}\text{C}$  that has better efficiency is at  $T_{\text{lamps}} = 440^{\circ}\text{C}$  (1). We conclude that  $T_{\text{RbF}} = 555^{\circ}\text{C}$  is an upper boundary for improving device performance with PDT. Not as many data points were obtained to determine the lower boundary of  $T_{\text{RbF}}$ . However, when looking at  $T_{\text{lamps}} = 460^{\circ}\text{C}$ , the sample at  $T_{\text{RbF}} = 495^{\circ}\text{C}$  does not show improvement over related baseline devices whereas the sample at  $T_{\text{RbF}} = 505^{\circ}\text{C}$  does. Although the  $T_{\text{RbF}}$  range may be convoluted with  $T_{\text{lamps}}$ , we estimate the range of  $T_{\text{RbF}}$  for successful RbF PDT, meaning that the RbF-PDT devices perform better than baseline devices, to be  $505^{\circ}\text{C}$  to  $555^{\circ}\text{C}$ .

$T_{\text{lamps}}$ , which directly correlates to substrate temperature during PDT, also influences the effectiveness of PDTs. If we look at  $T_{\text{RbF}} = 540^{\circ}\text{C}$  from left to right in Figure 2, the maximum device efficiencies start low, increase to a maximum at  $T_{\text{lamps}} = 460^{\circ}\text{C}$  (4), and then begin to decrease with increasing lamp setpoint temperature. The leftmost point ( $T_{\text{RbF}} = 540^{\circ}\text{C}$  and  $T_{\text{lamps}} = 380^{\circ}\text{C}$ ) was not an improvement over comparable baseline device performance. On the right side of the graph and according to the device efficiency, it appears that at  $T_{\text{RbF}} = 540^{\circ}\text{C}$ ,  $T_{\text{lamps}} = 560^{\circ}\text{C}$  is too high. Therefore, the  $T_{\text{lamps}}$  temperature for successful RbF PDTs is in the range of  $400^{\circ}\text{C}$  to  $540^{\circ}\text{C}$ .

### 3.3 Effects of Excess RbF During PDT

In addition to studying JV curves, we performed IVT on selected devices. Figure 4(a) displays dark IVT data for  $T_{\text{RbF}} = 540^{\circ}\text{C}$  and  $T_{\text{lamps}} = 460^{\circ}\text{C}$ , the point labeled 4 in Figure 2. The device has no evidence of blocking behavior. The device shown in (b) for  $T_{\text{RbF}} = 560^{\circ}\text{C}$  and  $T_{\text{lamps}} = 460^{\circ}\text{C}$  (2) does show an injection current barrier at low temperatures similar to that seen by Weiss et al. [7]. They found that if too much Rb is incorporated during a PDT, then the device fill factor suffers, presumably due to a surface layer created during the RbF PDT. In their study, higher RbF source temperature and higher substrate temperature increased the height of the barrier. Blocking behavior was not seen in IVT for the device at (5) in Figure 2 ( $T_{\text{RbF}} = 540^{\circ}\text{C}$  and  $T_{\text{lamps}} = 520^{\circ}\text{C}$ ). The IVT results and the improvement over baseline device performance support its inclusion in the process space for successful RbF PDT.

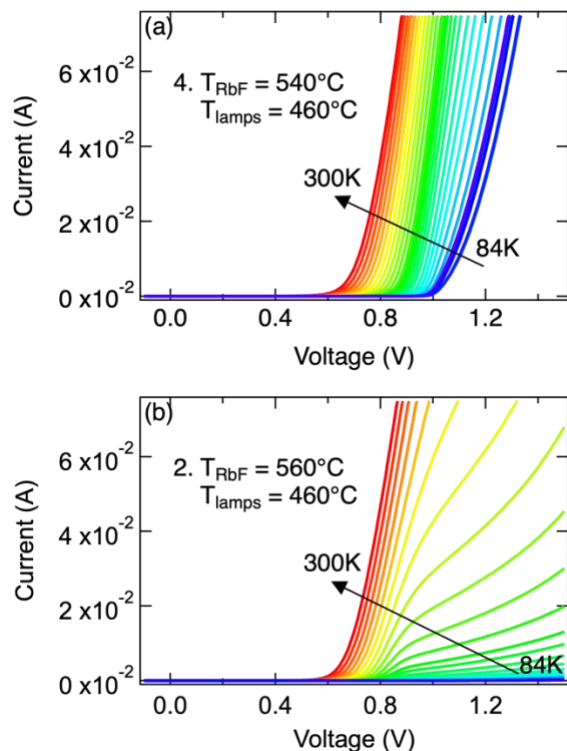


Figure 4. IVT graphs of devices with RbF PDTs. (a) is a high-efficiency device. (b) has lower efficiency and shows evidence of a current barrier, indicating that an excess of RbF was deposited during the PDT.

SIMS depth profiles confirm that higher  $T_{\text{RbF}}$  results in higher Rb concentration in the CIGS films. Three example SIMS profiles of ammonia-rinsed CIGS surfaces are shown in Figure 5(a). The red dashed line shows a very high  $T_{\text{RbF}} = 605^\circ\text{C}$ . In this case, a high concentration of Rb appears near the surface of the film. This is consistent with other reports of excess Rb on the surface and supports the hypothesis that a Rb-containing layer forms on the CIGS surface [6,8,13]. It also has a high average Rb concentration through the film of  $2.0 \times 10^{19} \text{ cm}^{-3}$ . A SIMS profile for  $T_{\text{RbF}} = 540^\circ\text{C}$  is shown by the green line. This corresponds to the conditions for the best device improvement with RbF PDT (4). It does not have the Rb build-up on the CIGS surface and has average Rb concentration of  $8.4 \times 10^{18} \text{ cm}^{-3}$ . For comparison, a sample with no intentional Rb added (No PDT) is also shown (blue dash dot). Some Rb was found in the film, likely due to contamination in the deposition system, but it was over 1.5 orders of magnitude lower than that found in the best PDT films.

Average Rb concentrations were calculated from the SIMS profiles by using the center flat regions of the curves, corresponding to the bulk of the CIGS film, and ignoring the buildup at the front surface and the back interface between the CIGS and Mo. Figure 5(b) shows average Rb concentrations versus RbF cell temperature for several example films. Clearly, average Rb concentrations in the films increase with increasing RbF cell temperature. When two points on the graph are at the same  $T_{\text{RbF}}$ , for example at  $T_{\text{RbF}} = 550^\circ\text{C}$ , then they are at different  $T_{\text{lamps}}$ . The lower  $T_{\text{lamps}}$  correspond to slightly higher average Rb concentration in both of those cases. We also looked at average Rb concentration versus lamp setpoint temperature as shown in Figure

5(c). A trend exists in this case as well, with average Rb concentration in the films decreasing with increasing Lamp Setpoint Temp. The Rb concentrations on this graph are influenced by the  $T_{RbF}$  as shown in Figure 5(b), so we conclude that the most important factor for the RbF PDT is the  $T_{RbF}$ , followed by the  $T_{lamps}$ .

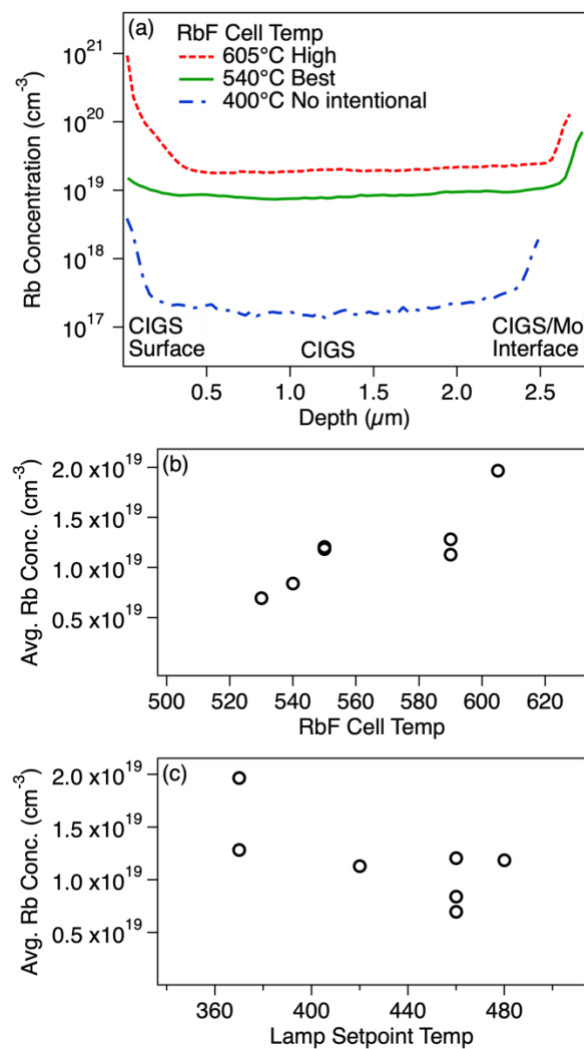


Figure 5. SIMS depth profiles (a) from samples with different RbF cell temperatures. High (red dash), best (green), and no intentional RbF deposition (blue dash-dot) are shown. Average Rb concentration versus RbF cell temperature (b) and lamp setpoint temperature (c).

### 3.4 The Best RbF PDT Recipe

The parameters for NREL's best RbF PDT recipe are shown in Table 4. The RbF cell temperature is 540°C and the lamp setpoint temperature is 460°C. The recipe followed the temperature profile shown in Figure 1 and described in the Experimental section. We have included the sample rinse information in the table as well. It is still possible that variations in absorber deposition processes or system configuration may make it difficult to exactly reproduce our results, like we had difficulty reproducing the results of other groups. The best RbF PDT increased the  $V_{oc}$  and FF of devices resulting in an increase in device efficiency. The average FF

increased by 0.5% absolute. Looking at  $V_{OC}$  alone in Figure 6(a) suggests that average gains are 30 to 40 mV between the samples without PDT (red squares) and with RbF PDT (blue circles). The data is split into two sets, side A and side B, because  $V_{OC}$ s are generally higher on side B of our samples compared to side A. Sample side variations occur because the system configuration has indium on one side and gallium on the other and it lacks sample rotation. We also found that the bandgap determined from quantum efficiency measurements increased slightly due to the RbF PDT Figure 6(b). To account for both effects when comparing  $V_{OC}$  between devices with and without RbF PDT, we used the difference between the bandgap ( $E_g$ ) divided by the elementary charge ( $q$ ) and the  $V_{OC}$ , rather than the  $V_{OC}$  alone. An example of this comparison is shown in Figure 7 where red squares are averages for devices with no PDT and blue circles are averages for devices with RbF PDT. Notice that the difference between  $E_g/q$  and  $V_{OC}$  is lower for the RbF PDT samples. That means they were closer to reaching the  $V_{OC}$  that is possible for their bandgap. The five points for each sample type are five individual growth runs, and each point represents at least 10 devices from each run. Some variation existed from run to run, which is another reason that the  $E_g/q$ - $V_{OC}$  comparison makes sense. The average for each sample type is shown by a dotted horizontal line and the values are given at the top of each column. For this set of devices, a 26-mV average gain in  $V_{OC}$  was achieved by implementing the RbF PDT.

Table 4. NREL Parameters for RbF PDT

Absorber Processing Method	Lamp Temp (°C)	Sample Temp (°C)	RbF Cell Temp (°C)	RbF Time	Dwell Time	Se Rate	Rinse Solution	Rinse Time, Temp
Three-stage coevaporation	460	445	540	4 min	9 min	25 Å/s	1.6 M NH <sub>4</sub> OH	4 min, 65 °C

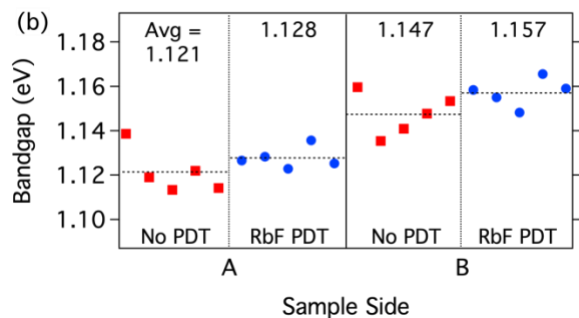
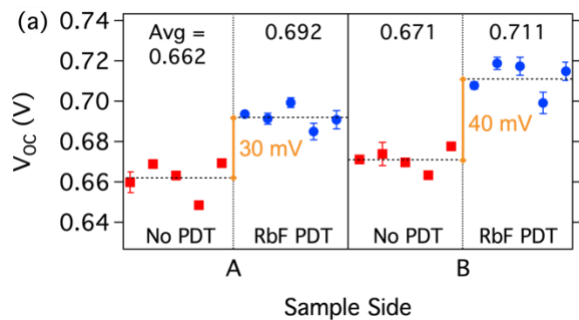


Figure 6.  $V_{oc}$  (a) and bandgap (b) for five samples with no PDT (red squares) and five samples with RbF PDT (blue circles). The data is split by sample side because of known compositional variation across the samples. Averages for each set are shown by dotted horizontal lines.

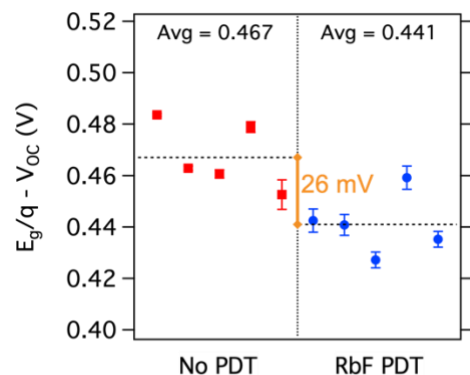


Figure 7. Difference between bandgap and  $V_{oc}$  for samples without (red squares) and with RbF PDT (blue circles). On average there is a 26 mV increase in  $V_{oc}$  for samples with the RbF PDT.

#### 4. Conclusion

RbF post-deposition treatment of CIGS was more difficult to optimize than KF post-deposition treatment. We varied the RbF cell and lamp setpoint over a wide range of temperatures and were able to set boundaries for successful RbF PDTs. RbF cell temperatures from 505°C through 555°C and lamp setpoint temperature from 400°C through 540°C produce devices that are better than their counterparts without RbF. The importance of RbF PDT parameters from most to least is RbF cell temperature, lamp setpoint (substrate) temperature, and Se flux. The best RbF PDT recipe was ultimately found for our system using  $T_{RbF} = 540^{\circ}\text{C}$  and  $T_{lamps} = 460^{\circ}\text{C}$ , and a description of the process is in the Experimental section. All the parameters, which are somewhat different from other recipes reported in the literature (Table 1), are shown in Table 4.

#### Acknowledgements

This work was authored by the National Renewable Energy Laboratory, operated by Alliance for Sustainable Energy, LLC, for the U.S. Department of Energy (DOE) under Contract No. DE-AC36-08GO28308. This material is based upon work supported by the U.S. Department of Energy's Office of Energy Efficiency and Renewable Energy (EERE) under the Solar Energy Technologies Office Award Number 34352. The views expressed in the article do not necessarily represent the views of the DOE or the U.S. Government. The U.S. Government retains and the publisher, by accepting the article for publication, acknowledges that the U.S. Government retains a nonexclusive, paid-up, irrevocable, worldwide license to publish or reproduce the published form of this work, or allow others to do so, for U.S. Government purposes.

#### References

- [1] P. Jackson, R. Wuerz, D. Hariskos, E. Lotter, W. Witte, M. Powalla, Effects of heavy alkali elements in  $\text{Cu}(\text{In,Ga})\text{Se}_2$  solar cells with efficiencies up to 22.6%, *Phys. Status Solidi RRL – Rapid Res. Lett.* 10 (2016) 583–586. <https://doi.org/10.1002/pssr.201600199>.

- [2] E. Avancini, R. Carron, T.P. Weiss, C. Andres, M. Bürki, C. Schreiner, R. Figi, Y.E. Romanyuk, S. Buecheler, A.N. Tiwari, Effects of Rubidium Fluoride and Potassium Fluoride Postdeposition Treatments on Cu(In,Ga)Se<sub>2</sub> Thin Films and Solar Cell Performance, *Chem. Mater.* 29 (2017) 9695–9704. <https://doi.org/10.1021/acs.chemmater.7b03412>.
- [3] J.M. Raguse, C.P. Muzzillo, J.R. Sites, L. Mansfield, Effects of Sodium and Potassium on the Photovoltaic Performance of CIGS Solar Cells, *IEEE J. Photovolt.* 7 (2017) 303–306. <https://doi.org/10.1109/JPHOTOV.2016.2621343>.
- [4] L.M. Mansfield, R. Noufi, C.P. Muzzillo, C. DeHart, K. Bowers, B. To, J.W. Pankow, R.C. Reedy, K. Ramanathan, Enhanced Performance in Cu(In,Ga)Se<sub>2</sub> Solar Cells Fabricated by the Two-Step Selenization Process With a Potassium Fluoride Postdeposition Treatment, *IEEE J. Photovolt.* 4 (2014) 1650–1654. <https://doi.org/10.1109/JPHOTOV.2014.2354259>.
- [5] M. Mezher, L.M. Mansfield, K. Horsley, M. Blum, R. Wieting, L. Weinhardt, K. Ramanathan, C. Heske, KF post-deposition treatment of industrial Cu(In, Ga)(S, Se)<sub>2</sub> thin-film surfaces: Modifying the chemical and electronic structure, *Appl. Phys. Lett.* 111 (2017) 071601. <https://doi.org/10.1063/1.4998445>.
- [6] S. Ishizuka, N. Taguchi, J. Nishinaga, Y. Kamikawa, S. Tanaka, H. Shibata, Group III Elemental Composition Dependence of RbF Postdeposition Treatment Effects on Cu(In,Ga)Se<sub>2</sub> Thin Films and Solar Cells, *J. Phys. Chem. C.* 122 (2018) 3809–3817. <https://doi.org/10.1021/acs.jpcc.8b00079>.
- [7] T.P. Weiss, S. Nishiwaki, B. Bissig, R. Carron, E. Avancini, J. Löckinger, S. Buecheler, A.N. Tiwari, Injection Current Barrier Formation for RbF Postdeposition-Treated Cu(In,Ga)Se<sub>2</sub>-Based Solar Cells, *Adv. Mater. Interfaces.* 5 (2018) 1701007. <https://doi.org/10.1002/admi.201701007>.
- [8] T. Kodalle, M.D. Heinemann, D. Greiner, H.A. Yetkin, M. Klupsch, C. Li, P.A. van Aken, I. Lauer mann, R. Schlatmann, C.A. Kaufmann, Elucidating the Mechanism of an RbF Post Deposition Treatment in CIGS Thin Film Solar Cells, *Sol. RRL.* 2 (2018) 1800156. <https://doi.org/10.1002/solr.201800156>.
- [9] S. Karki, S. Marsillac, P. Paul, G. Rajan, B. Belfore, D. Poudel, A. Rockett, E. Danilov, F. Castellano, A. Arehart, Analysis of Recombination Mechanisms in RbF-Treated CIGS Solar Cells, *IEEE J. Photovolt.* 9 (2019) 313–318. <https://doi.org/10.1109/JPHOTOV.2018.2877596>.
- [10] US Patent No. 5,441,897 (15 August) and US Patent No. 5,436,204 (25 July), 1995.
- [11] M.A. Contreras, M.J. Romero, B. To, F. Hasoon, R. Noufi, S. Ward, K. Ramanathan, Optimization of CBD CdS process in high-efficiency Cu(In,Ga)Se<sub>2</sub>-based solar cells, *Thin Solid Films.* 403–404 (2002) 204–211. [https://doi.org/10.1016/S0040-6090\(01\)01538-3](https://doi.org/10.1016/S0040-6090(01)01538-3).
- [12] I. Repins, S. Glynn, J. Duenow, T.J. Coutts, W.K. Metzger, M.A. Contreras, Required material properties for high-efficiency CIGS modules, in: A.E. Delahoy, L.A. Eldada (Eds.), San Diego, CA, 2009: p. 74090M. <https://doi.org/10.1117/12.828365>.
- [13] S. Ishizuka, N. Taguchi, P.J. Fons, Similarities and Critical Differences in Heavy Alkali-Metal Rubidium and Cesium Effects on Chalcopyrite Cu(In,Ga)Se<sub>2</sub> Thin-Film Solar Cells, *J. Phys. Chem. C.* 123 (2019) 17757–17764. <https://doi.org/10.1021/acs.jpcc.9b06042>.

